



Investigation of Microstructural Textures in Al–TiAl₃ Nanocomposites Fabricated Through Cold Roll Bonding–Annealing–ARB and Cold Roll Bonding–ARB–Annealing Processes

Zohreh Yazdani¹ · Mohammad Reza Toroghinejad¹ · Hossein Edris¹

Received: 27 April 2022 / Accepted: 13 March 2023 / Published online: 29 March 2023
© Indian National Academy of Engineering 2023

Abstract

This paper investigates the texture of Al–TiAl₃ nanocomposites prepared by two different processes. First, a sandwich of two Al sheets with Ti powder underwent CRB. Subsequently, two groups of annealed-ARB and ARB-annealed samples were prepared. Microstructural texture was investigated by TEM, EBSD, and ODF analysis. Results showed a decrease in intensity of the cube component because of formation of nano shear bands in the fifth cycle of ARB. It was found that the presence of large particles of intermetallic compounds completely changes the annealing texture by affecting the movement of boundaries. With increase in the number of ARB cycles after annealing, the recrystallization texture components were completely eliminated. Only the deformation texture components, including strong Goss, Copper, Dillamore, Brass, and S components, were present. A remarkable point was the elimination of the cube texture component in the structure after the third cycle of ARB due to the development of shear bands.

Keywords Ti aluminide · Accumulative roll bonding · Metal matrix nanocomposite · Intermetallic compounds · TiAl₃ · Texture

Introduction

In recent years, Al metal matrix composites have received considerable attention due to their light weight, high elastic modulus, and suitable electrical and magnetic properties. They have many modern and advanced applications in aerospace, defense, and automotive industries (Rana et al. 2012). These composites consist of Ti–Al intermetallic compounds, and thus present a combination of the low density and high strength of Ti aluminides and high toughness of Ti or Al. Moreover, the high-temperature behavior of aluminides will be maintained by the composite (Heathcote et al. 1996; Lesuer and Syn 1994). One of the methods of fabricating

these composites is the cold roll bonding (CRB) process of Al–Ti, and then annealing treatment to form titanium aluminide compounds (Lesuer and Syn 1994). Accumulative roll bonding (ARB) procedure, as a severe plastic deformation method, has a remarkable capability to provide materials with nanometer grain size and unique properties such as high strength at ambient temperature, superplastic properties at high strain rates and low temperatures, as well as high corrosion resistance (Saito et al. 1998, 1999; Tsuji et al. 2002). In this process, the strain is distributed almost uniformly throughout the grains. The repetition of the process for a high number of cycles results in a uniform distribution of reinforcement particles in the matrix. This process involves roll bonding the sheets, halving them, and re-roll bonding. Repeating this process causes a relatively high strain in each layer in each cycle, thus causing severe plastic deformation throughout the sheet. In the ARB process, the occurrence of severe plastic deformation on multilayer materials and fine-graining leads to the development of geometrically necessary boundaries and incidental dislocation boundaries (Saito et al. 1998). In previous researches, roll bonding or ARB process, and then annealing treatment have mostly been used to produce Ti aluminide intermetallic compounds

✉ Zohreh Yazdani
z.yazdani@ma.iut.ac.ir

Mohammad Reza Toroghinejad
toroghi@cc.iut.ac.ir

Hossein Edris
h-edris@cc.iut.ac.ir

¹ Department of Materials Engineering, Isfahan University of Technology, Isfahan 84156-83111, Iran

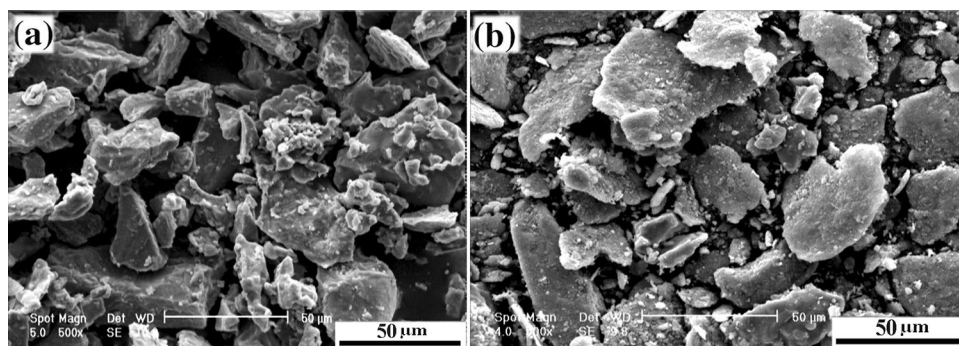
(Oh et al. 2003; Luo and Acoff 2004; Chaudhari and Acoff 2010; Sieber and Perepezko 2000; Yang et al. 2009; Loo and Rieck 1973). These researches have shown that increasing strain during rolling by creating crystal defects increases the rate of formation of intermetallic compounds in the subsequent annealing stage. However, under these circumstances, it is not possible to achieve a final product with small grain size and good mechanical properties. Recently, a different method has been applied to the layers of Al sheet/Ti powder/Al sheet, in which, first, annealing treatment is performed and intermetallic compounds are formed, and then ARB method is applied to distribute the reinforcement particles in the composite and to fine grain the structure (Yazdani et al. 2018a). In fact, in this method, the slip pattern of plastic deformation in areas close to the intermetallic compounds is dissimilar to other regions; thus, the geometrically necessary boundaries are established. These large misorientation angle boundaries are increased and also the strength is increased through a grain boundary strengthening mechanism (Liu et al. 2012). Therefore, it is essential to compare the properties of the composites obtained through these two different methods. Texture is among the properties that can be compared. Crystalline texture has a vital function in the physical and mechanical properties of materials. Materials that undergo roll bonding or ARB have many grains, each of which has a specific orientation with the rolling direction, which results in the formation of different texture components in the material. First, the deformation and recrystallization (or annealing) texture components of materials with face-centered cubic (FCC) lattice must be considered in three-dimensional Euler space. For cube crystals, the orientation of a crystal is determined using the $\{hkl\}\langle uvw \rangle$ Miller indices; $\{hkl\}$ corresponds to the Miller indices of a crystal plane parallel to the rolling plane, and $\langle uvw \rangle$ portrays the Miller indices of a direction of the crystal that is parallel to the rolling direction. The preferred orientation usually exists in the form of deformation and recrystallization textures. The texture can change throughout welding, plastic deformation, casting, and even annealing treatments. Texture changes in ARB specimens differ from that of specimens that are routinely roll bonded. Previously,

an increase in rolling texture components due to ARB and the configuration of equiaxed nanometer grains because of high shear strain has been reported in Al 1100 samples (Raei et al. 2010). Moreover, the effect of large secondary particles on deformation or annealing texture has been investigated. It has been shown, for example, that one of the impacts of the presence of secondary phase particles is increase in the intensity of the rotated cube texture component (Jamaati et al. 2011). The purpose of the present study was to fabricate an Al metal matrix nanocomposite with Ti aluminide reinforcement through the two methods of CRB–annealing treatment–ARB and CRB–ARB–annealing treatment to investigate the effect of the annealing stage or Ti aluminide intermetallic compounds fabrication stage before and after ARB on the microstructure and texture of the final product.

Materials and Methods

For the fabrication of Al/Ti aluminide composite, an Al 1100 sheet of $100 \times 50 \times 1 \text{ mm}^3$ was used. These sheets were annealed at $350 \text{ }^\circ\text{C}$ for 1 h to remove the roll bonding history in the material. Ti powder with 99% purity was obtained from Merck & Co. Kenilworth, NJ, USA. The SEM image of this powder is demonstrated in Fig. 1. As can be seen, this powder has inhomogeneous particle size distribution with an angular morphology (Fig. 1a). Due to the large particles of primary Ti powder and increased adhesion of powder particles during the roll bonding process, the primary Ti powder was subjected to mechanical ball milling for 7 h. Mechanical ball milling (Retsch PM100) was performed in a planetary ball mill at a disk rotation speed of 500 rpm. In all operations performed using this mill, five steel balls with a diameter of 2 cm and balls to powder weight ratio of 10:1 were used. According to Fig. 1b, due to mechanical ball milling, although the particle size distribution is still inhomogeneous, the size of Ti particles (average size: $45 \text{ }\mu\text{m}$) decreased and reached $0.8 \text{ }\mu\text{m}$. To perform the initial CRB cycle, the annealed Al sheets were cut to the dimensions of $100 \times 50 \times 1 \text{ mm}^2$, and the four corners of the sheets were perforated. After acid washing and cleaning with acetone,

Fig. 1 SEM image of primary Ti powder **a** before and **b** after ball milling for 7 h



they were brushed to establish a suitable connection between the Al layers, and a surface roughness of 3 μm was created. A wire brush with an outer diameter of 6 cm was selected for brushing. To apply Ti powder between Al sheets, the powder was poured into an ethanol solution, and then sprayed evenly onto the Al sheet surface. The holes were fixed with steel wire to prevent the sheets from moving during the roll bonding. After surface preparation of the samples, to prevent the re-contamination of the surfaces, the roll bonding procedure should be carried out for a duration of less than 120 s. Finally, CRB was implemented using a rolling machine with a rotation speed of 10 rpm. First, Al sandwiches containing 0.5 wt% of Ti were prepared, and then CRB was performed by 50% thickness reduction. The 50% thickness reduction was selected based on the previous work of these authors and the value of threshold thickness reduction in this system (Yazdani et al. 2018b). Annealing treatment of the samples was performed in an electric furnace at 590 °C for 2 h. To protect the samples from oxidation, they were placed in containers containing alumina powder. The samples were then cooled to room temperature at a heating rate of 10 °C/min, and finally, cooled in the furnace.

To perform the ARB process, the specimens were split in half, and subsequently, the two cut parts were brushed and stacked on top of each other. The four corners of the specimen were perforated and the sheets were tightly fixed with steel wires. Then CRB was performed on the samples with 50% deformation in each cycle. In the second cycle, the sample from the first cycle was divided into two equal parts, and after brushing, the samples were stacked on top of each other, and then rolled. The same process was followed in subsequent cycles. To prevent the spread of edge cracks created during cumulative rolling cycles, the cracked parts were cut after each cycle.

In the first fabrication method, several cold roll bonded sandwiches were annealed at 590 °C for 2 h. The basis for selecting this temperature and time to achieve the TiAl_3 intermetallic compounds in this system was the previous work in this regard (Yazdani et al. 2018a). The sample was then subjected to the ARB process for a maximum of five cycles. For convenience, the CRB abbreviation is used for the initial cold roll bonded sample, CRB–AT is used for the initial cold roll bonded, and then annealed sample, and the CRB–AT–ARB for the sample that underwent initial CRB, annealing, and then ARB. Some monolithic Al sandwiches without Ti powder were also prepared and produced using the same method. In this text, these samples are named Al–ARB samples.

In the second method of composite fabrication, a number of Al 1100 sheet sandwiches containing 0.5 wt% of titanium powder samples, after CRB, underwent a maximum of five cycles of ARB, and then were annealed at 590 °C for 2 h to form TiAl_3 intermetallic compounds. In this text, the

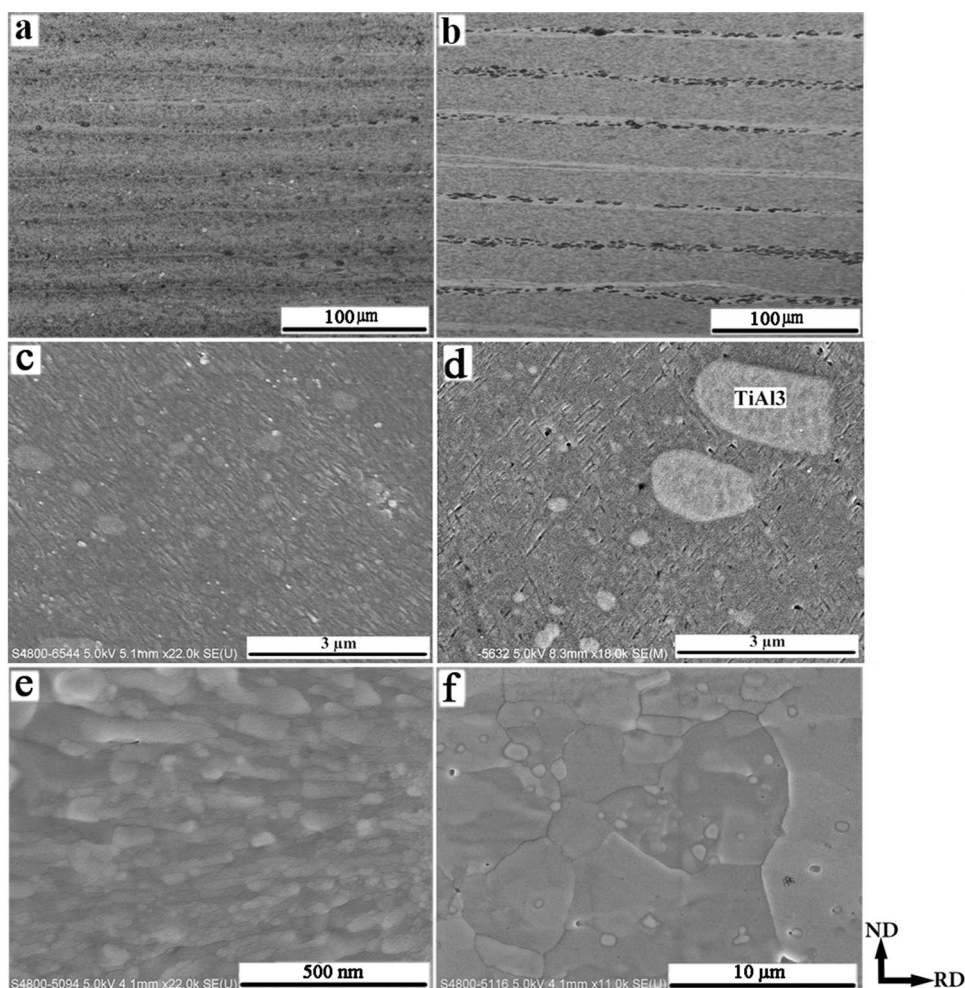
abbreviations of CRB, CRB–ARB, and CRB–ARB–AT are considered for samples which have undergone initial cold roll bonding, initial cold roll bonding, and then ARB, and initial cold roll bonding, ARB, and then annealing treatment, respectively.

To evaluate the microstructure of the obtained phases and the distribution of particles, a field emission scanning electron microscopy (FESEM) device (model S-4800; Hitachi, Chiyoda City, Tokyo, Japan) was used. The transmission electron microscopy (TEM) device (Tecnai G2 20 S-TWIN; FEI Company, Hillsboro, OR, USA) was employed for more detailed microstructural studies in different grains and grain boundaries, and nano-observations. An electropolishing device was used to prepare the samples for TEM microstructural examination. Another FESEM microscope (LEO 1530 FEG; ZEISS, Jena, Germany) was utilized to study the orientation of the grains. It was equipped with the electron backscatter diffraction (EBSD) analysis device to determine the microstructural texture of the samples. Sample preparation included hot mounting and polishing. To remove the deformed surface layers, the samples were subjected to vibration polishing containing 50 nm silica colloidal particles for 12 h after conventional polishing. The samples were then subjected to EBSD analysis. This analysis was performed at a voltage of 20 kV on the RD–ND plate at exactly half the thickness. The scanning step size used was determined based on sample type from within the range of 0.05–2 μm . The data obtained from the EBSD analysis detector were processed using JTEX software (Laboratories LEM3, Metz, France). Texture data were extracted after rotating 90 degrees around the RD axis. To determine the type of texture in different samples, the orientation distribution functions (ODF) were compared with the standard texture components, and the texture components were identified.

Results and Discussion

The microstructure evaluations of the CRB–AT–ARB5 and CRB–ARB5–AT samples are presented in Fig. 2. Figure 2a, b displays an overview of the final Al– TiAl_3 samples obtained using optical microscope images. Figure 2a shows a picture of the CRB–AT–ARB5 sample. According to this image, the final structure is in the form of a compact layer containing an ultra-fine grain Al matrix with a suitable distribution of TiAl_3 intermetallic compound particles. The optical microscope image of the CRB–ARB5–AT sample is presented in Fig. 2b. This image also presents the layer structure. A closer look reveals the presence of a recrystallized Al matrix enclosed in the particles of the TiAl_3 intermetallic compound at the interface. Reinforcement particles are mainly present in the interface layer, and

Fig. 2 **a** Optical image of the CRB–AT–ARB5 samples, **b** optical image of the CRB–ARB5–AT sample, and FESEM images at different magnifications: **c, e** CRB–AT–ARB5 sample, and **d, f** CRB–ARB5–AT sample



therefore have a less uniform distribution than that in the CRB–AT–ARB5 sample (Fig. 2a). In general, the ARB process has led to the distribution of intermetallic compound particles in the CRB–AT–ARB sample and the distribution of Ti particles in the CRB–ARB–AT sample. The principal goal of applying the ARB method in the next step is the breakup of the particles and their even distribution in the Al matrix. FESEM images of these two samples that mainly show the size and shape of particles can be seen in Fig. 2c, d. In the CRB–AT–ARB5 sample in Fig. 2c, continuous plastic deformation in the ARB method, the suitable distribution of particles, and the breakup of particles eliminated the Kirkendall voids created during intermetallic compound formation and enhance the mechanical properties of the material. As evidenced, with ARB, the intermetallic compound particles break up due to the vertical compressive force of the roller and the increase in the length of the rolled sheets, and a better dispersion is seen in the particles. Moreover, a good distribution of particles with a size greater than 200 nm is observed in the microstructure. Furthermore, Kirkendall voids are not visible at this scale. Reducing the number of

voids enhances the bonding quality between the intermetallic compound particles and the bonding quality between the two Al sheets and ultimately enhances the strength of the composite (Jamaati and Toroghinejad 2010). Figure 2d is related to the second fabrication method in which the specimen underwent CRB, ARB, and then annealing. According to 2-d, annealing results of the CRB–ARB sample, which underwent five ARB cycles, show that the particle size of the intermetallic compound has decreased due to the increase in the number of ARB cycles. However, due to the presence of large Ti particles after five ARB cycles, the intermetallic TiAl_3 compound is present in different sizes in the microstructure. According to these images, after five cycles of ARB and annealing, fine intermetallic composite particles as small as 200 nm along with large micron particles are present in the microstructure. The morphology of the smaller particles is also very close to spherical. The FESEM images of the Al matrix obtained at higher magnification in the CRB–AT–ARB5 sample and the CRB–ARB5–AT sample are shown in Fig. 2e, f. Examination of these images confirms that a maximum of five cycles of ARB after annealing

(Fig. 2e) has led to the extension of the lamellar structure of nanometer thickness within the Al matrix in the rolling direction. In contrast, annealing after ARB (Fig. 2f) has resulted in a dual recrystallized structure of Al with large grains (maximum size of 30 μm). Plastic deformation leads to significant structural changes such as grain size variations, strain hardening, and increased dislocation densities. Moreover, annealing treatment changes the morphology of the grains. It increases the grain size and the softening of the matrix through the returning processes of recovery, recrystallization, and grain growth. The fine-graining mechanism also largely depends on the rolling process. Increasing the dislocation densities is one of the main tools of fine graining in the ARB process. In addition, in the case of annealing after rolling, recrystallization is the main fine-graining mechanism. This is in line with previous reports (Zhang et al. 2017; Zhao et al. 2016).

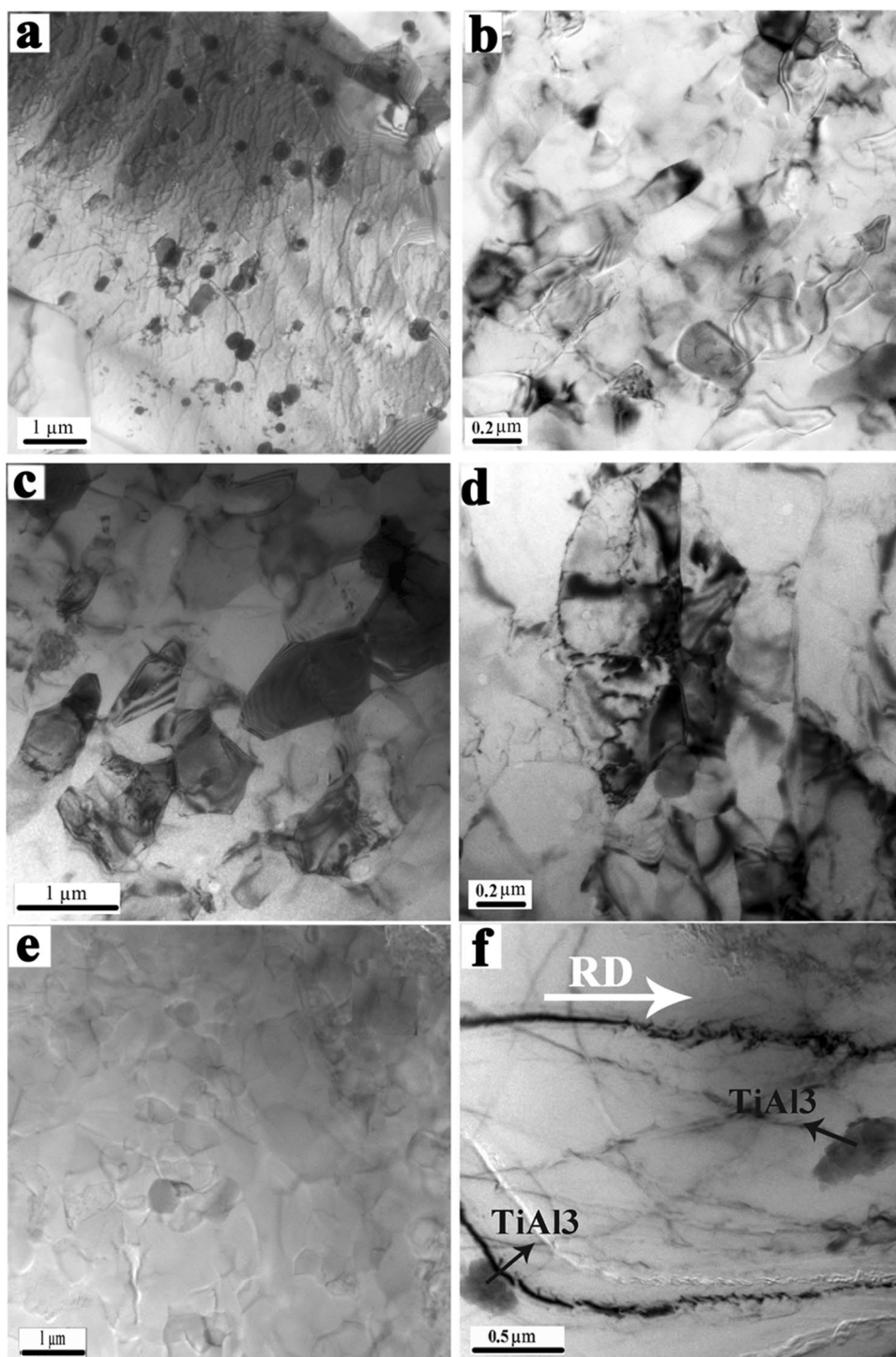
Figure 3 illustrates the TEM images of CRB–AT–ARB5, Al–ARB5, and CRB–ARB5–AT samples. TEM images of the microstructure of the CRB–AT–ARB5 composite with a strain equivalent to 4 are shown in Fig. 3a, b. Figure 3a clearly shows the uniform dispersion of the intermetallic compound particles. According to Fig. 3b, after five ARB cycles, the dislocation densities increased, the dislocations within the cells decreased, and the sub-grains became smaller. The sub-grain size of the Al matrix is at most 500 nm. As the number of ARB cycles increased, the misorientation in the low-angle boundaries of the sub-grains and cellular structures, and the percentage of ultra-fine grain regions also increased. Moreover, the particle size of the intermetallic compound has reached about 200 nm. This image confirms the formation of sub-grains around the intermetallic compound particles. TEM images of the Al–ARB5 sample are presented in Fig. 3c, d. It can be observed that, in this sample, the grain size of Al declined with increase in the number of ARB cycles, and finally, a structure containing grains of sub-micron size was obtained. It can be seen that more fine graining has occurred in the composite sample than in the monolithic Al sample. In fact, in the composite sample, there is more grain refining in the particle–matrix interfaces caused by particles. Therefore, finely dispersed intermetallic particles can increase the dislocation density and reduce the grain size in the structure of the Al matrix. TEM images of the CRB–ARB5–AT sample are shown in Fig. 3e, f. According to this figure, due to the annealing of the sample after five cycles of ARB, the processes of recovery and elimination of dislocations and, in some parts of the microstructure, recrystallization, and grain growth of Al have occurred. In this sample, the Al grain size is significantly increased. In some areas, the formation of equiaxed grains is observed due to the recrystallization process (Fig. 3e). In others, the presence of columnar grains due to deformation with grain boundaries stretched in the rolling

direction (Fig. 3f) is observed. The reduction in the number of sub-grains within these columnar grains is also clearly seen due to annealing. The presence of sub-micron-sized TiAl_3 intermetallic particles is indicated in this figure. The energy-dispersive X-ray spectroscopy (EDS) analysis of the TEM image related to one of the specified particles in Fig. 3f was measured and the percentage of elements, which is shown in Fig. 4, was calculated. EDS analysis confirmed the presence of the TiAl_3 compound. Therefore, it can be said that after five ARB cycles, both types of composites have produced an Al matrix composite with evenly dispersed TiAl_3 reinforcement particles.

EBSD test results were used to evaluate the crystalline texture. Important texture components commonly formed due to rolling in these materials include Goss, Copper, Brass, Dillamore, Cube, and S $\{123\}\langle 634\rangle$ components. Furthermore, the annealing of Al sheets can result in considerable changes in texture, including the development of a cube texture, the appearance of a texture similar to a rolling texture, the formation of one or more new texture components, and the development of random texture (Humphreys and Hatherly 2004). In this study, annealing caused several new recrystallization texture components called P ($\{011\}\langle 122\rangle$), Q ($\{013\}\langle 231\rangle$), R ($\{124\}\langle 211\rangle$), and R5 ($\{852\}\langle 524\rangle$). ODF also provide an excellent opportunity to analyze texture changes in more detail. These functions can be used to quantify textures in terms of a small number of principal components. Images from φ_2 sections of 45° , 65° , and 90° are usually used to examine rolling texture because they contain all the components of the FCC deformation texture. The demonstration components of rolling in these sections are shown in Fig. 5.

Pole figure images of (111) plane and corresponding ODF in φ_2 sections equal to 45° , 65° , and 90° related to the initial Al, CRB, CRB–AT samples after the first, third, and fifth cycles of ARB (CRB–AT–ARB1, CRB–AT–ARB3, and ACRB–AT–ARB5) are shown in Figs. 6 and 8, respectively. It should be noted that the pole figure and corresponding ODF images are measured at half the thickness of the sheet. The position of some important texture components is shown in the pole figure images. However, due to the overlap or proximity of different components in pole figure images, it is not possible to determine the exact intensification of the components, and to do this, the ODF results must be used. Figure 6a shows that the initial Al has R5 and Q recrystallization texture components. It also contains rolling texture S, which is related to the deformation effects of initial Al before annealing. According to Fig. 7a, the ODF images of the initial Al specimen confirm the presence of recrystallization texture. The (111) pole figure image of the CRB specimen in Fig. 6b shows the formation of a rolling texture containing Copper and Goss components. The S component is also amplified in this image. Among the recrystallization

Fig. 3 TEM images of **a, b** CRB–AT–ARB5 sample, **c, d** Al–ARB5 sample, and **e, f** CRB–ARB5–AT sample at different magnifications



texture components, only the R5 recrystallization component is present after CRB with a slight decrease in intensity. The ODF images of this sample, according to Fig. 7b, show the formation of the Goss component, one of the components of α fiber (in the section φ_2 equal to 90°). According to Fig. 6c, annealing after CRB (CRB–AT) has led to the strengthening of the recrystallization texture. In this case, in addition to components R5 and R, another strong element

(P) is present in the recrystallization texture. This change in annealing texture relative to the initial Al is because of the existence of large Ti aluminide particles. The appearance of second particles completely changes the annealing texture by affecting the movement of the grain boundaries (Humphreys and Hatherly 2004). The ODF images of this sample show the disappearance of the rolling texture components and the formation of areas with recrystallization texture

Fig. 4 EDS analysis of the TEM image of particles in Fig. 3f

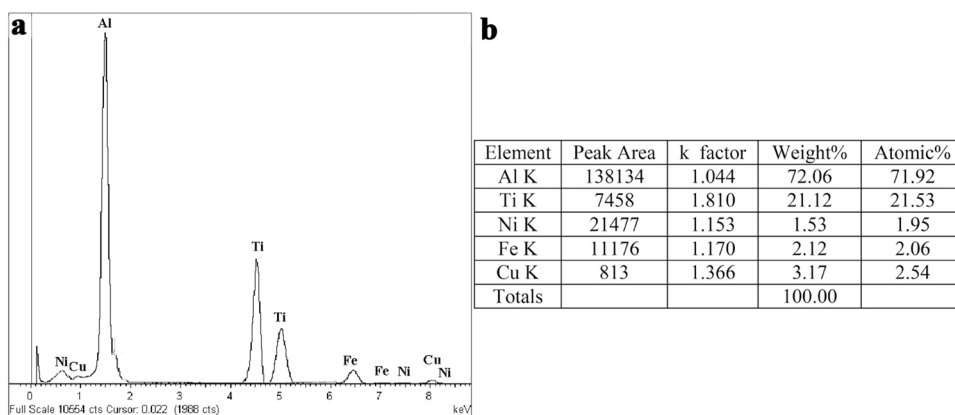
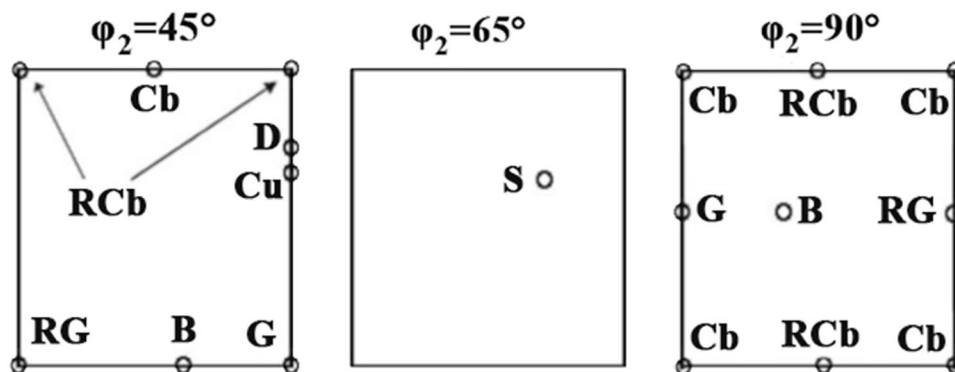


Fig. 5 Schematic of important component positions in rolling materials with FCC structure in ϕ_2 sections equal to 45° , 65° , and 90° : Copper (Cu), Cube (Cb), Brass (B), Dillamore (D), Rotated Cube (RCb), Goss (G), S and Rotated Goss (RG)



(Fig. 7c). In addition, the intensity of the fibers decreases due to annealing. Moreover, the partial appearance of the cube texture component due to the annealing treatment can also be seen in this image. The (111) pole figure image of the CRB–AT–ARB1 sample is presented in Fig. 6d. Due to the ARB process, the development of rolling texture components, including the Copper, Goss, Dillamore, and S components, is clearly visible. Furthermore, prominent recrystallization components in this sample are the Q and R components. During recrystallization, the preferred orientation which was formed by cold work transforms into a completely other preferred orientation. In fact, nuclei of various orientations initially form, but because the rate of growth of any given nucleus depends on the orientation difference between the matrix and growing crystal, the recrystallized texture will develop from those nuclei that have the fastest growth rate in the cold-worked matrix, i.e., those bounded by large angle boundaries (Smallman and Bishop 1999). The ODF images of this sample, shown in Fig. 7d, are very similar to that of the CRB (8-b) sample, except that the recrystallization components resulting from the annealing treatment are still intense due to the relatively high annealing temperature. However, the rolling components of Goss and Copper are formed after one cycle of ARB. None of α and β fibers are formed in this sample. Another point is that with increase in strain, the cube component is slightly strengthened. As

shown in Fig. 6e, the CRB–AT–ARB3 sample contains the rolling texture components of Copper, Goss, and S. However, in this sample, the Brass component is also formed. Moreover, the recrystallization components R and R5 are still present. Furthermore, with the formation of the Brass component, according to Fig. 7e, in sections ϕ_2 equal to 45° and 90° , the α fiber, which is the connection of the Gauss (G) and Brass (B) components, has been formed. In addition, in these ODF sections, as the strain raises, the intensity of the rotated cube component also increases. Finally, the pole figure image of the CRB–AT–ARB5 sample is shown in Fig. 6f. According to this image, the recrystallization texture components have been completely removed, and only the deformation texture components, including the Goss, Copper, Dillamore, Brass, and S components, are present. The Brass component is also strengthened by rolling. However, there is no trace of the presence of a cube component. The ODF images in Fig. 7f show that in addition to amplifying α fiber, the β fiber is also formed. The β fiber starts from the Copper component, then extends to the S component, and finally, to the Brass component. However, the rotated cube component has been eliminated in this sample. In general, α and β fibers are quickly formed in metals with high stacking faults energy, such as Al and Cu. Moreover, as the amount of deformation increases, α fiber and the Goss component are strengthened. It was observed that by performing ARB,

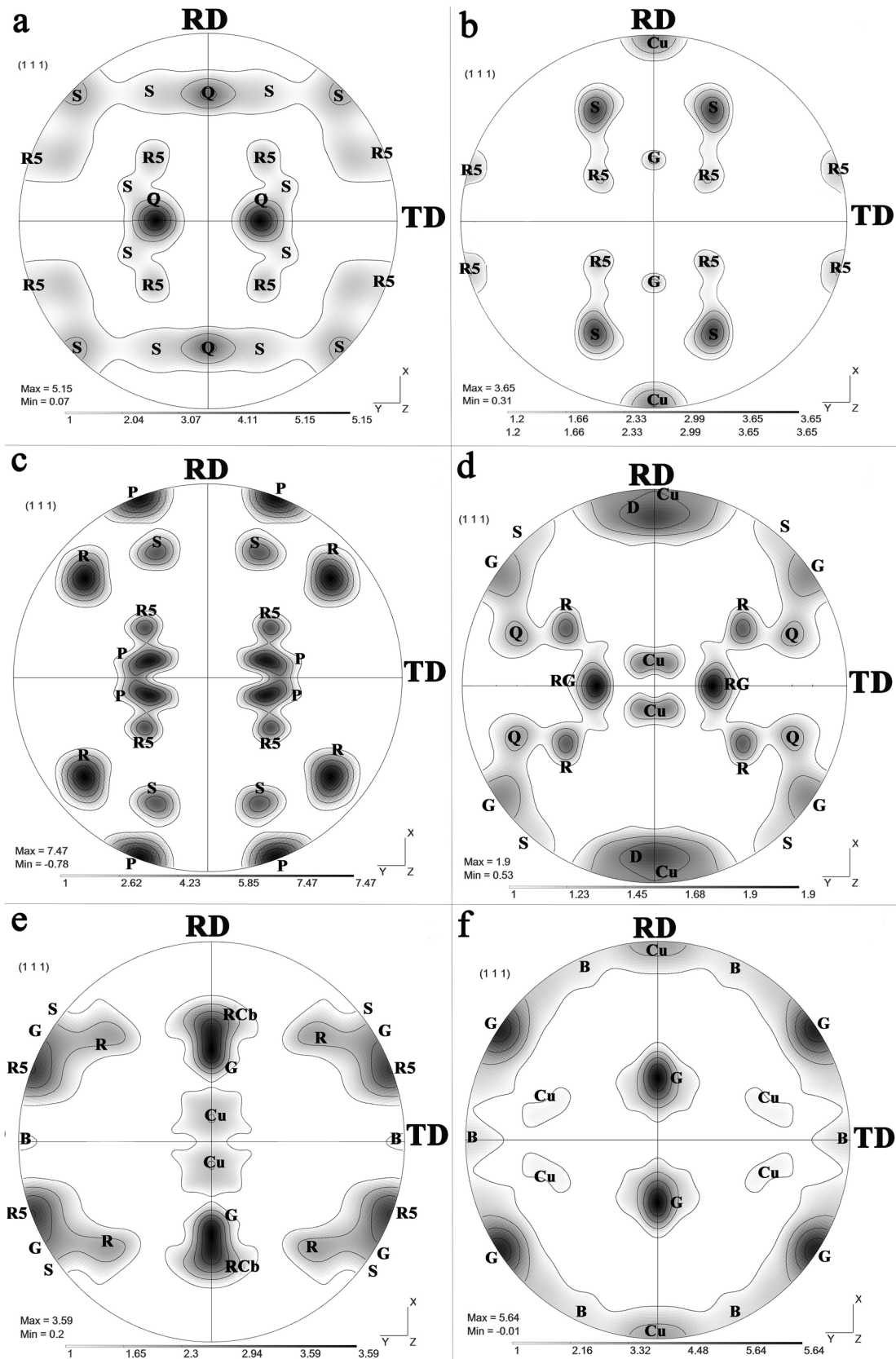


Fig. 6 (111) pole figure images of the RD-TD section obtained from EBSD test related to **a** initial Al, and **b** CRB, **c** CRB-AT, **d** CRB-AT-ARB1, **e** CRB-AT-ARB3, and **f** CRB-AT-ARB5 samples

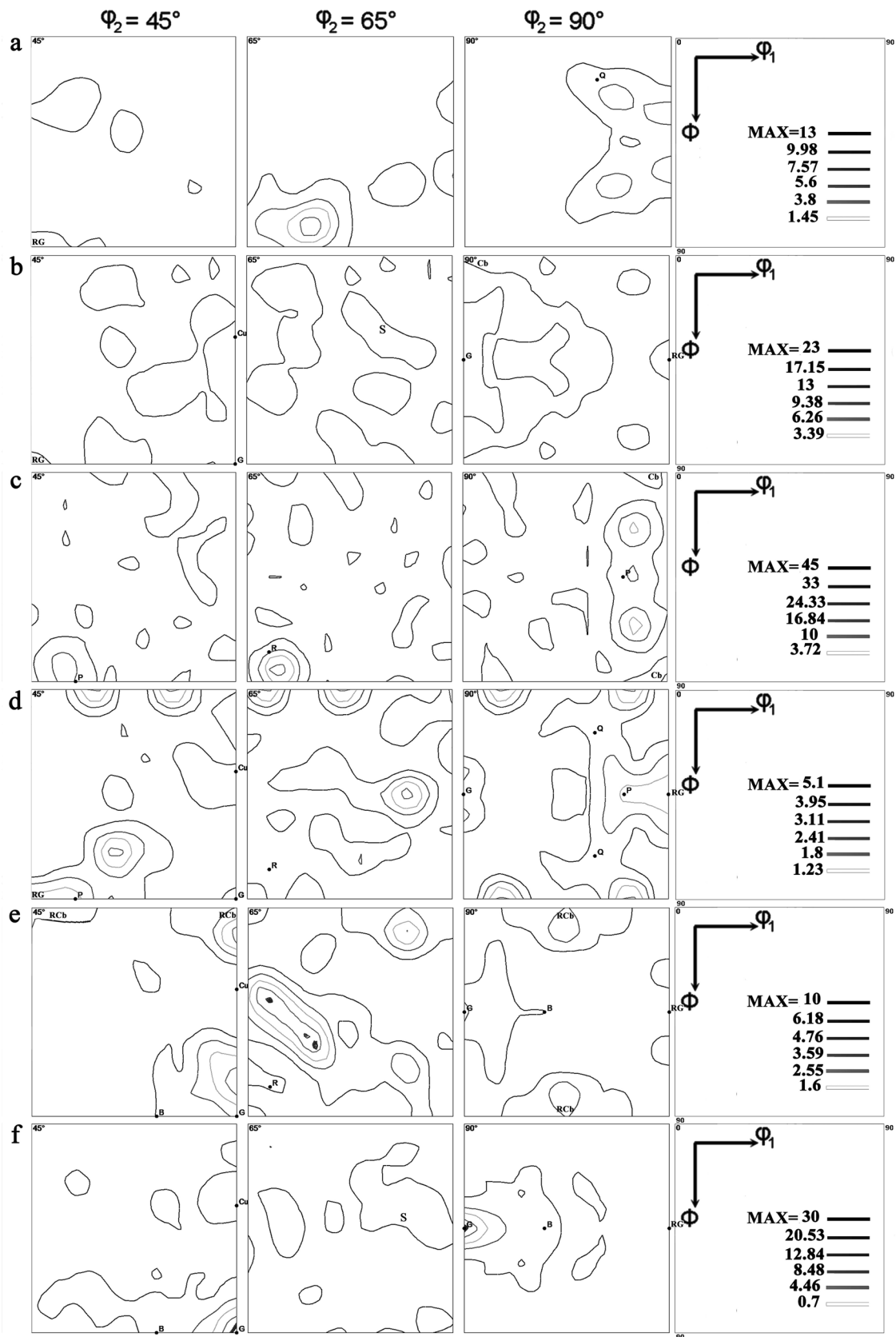
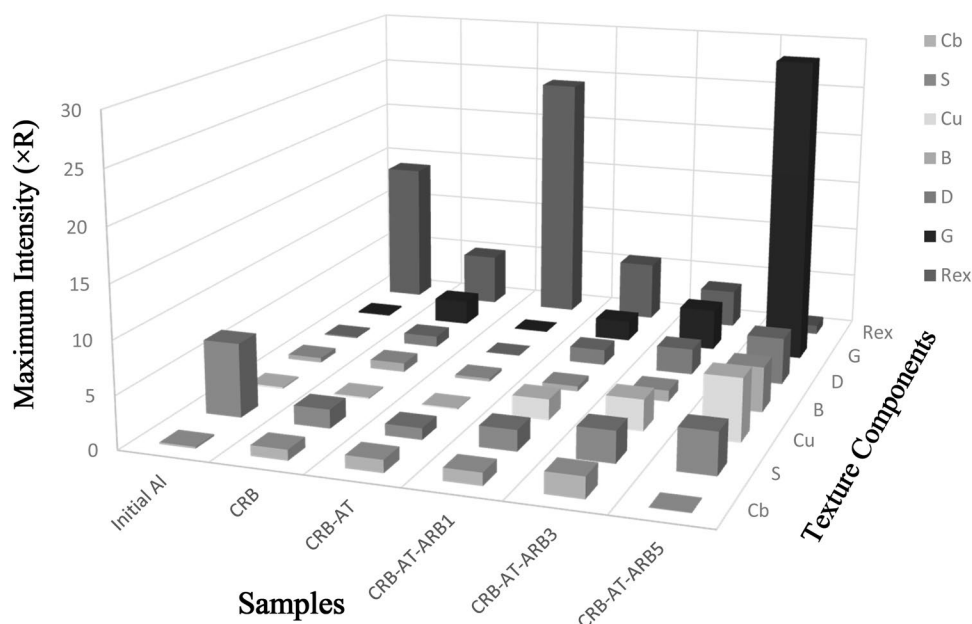


Fig. 7 ODF images in sections ϕ_2 equal to 45° , 65° , and 90° in the RD-TD plane obtained from EBSD test in **a** initial Al, and **b** CRB, **c** CRB-AT, **d** CRB-AT-ARB1, **e** CRB-AT-ARB3, and **f** CRB-AT-ARB5 samples

Fig. 8 Values of important texture components in initial Al, and CRB, CRB–AT, CRB–AT–ARB1, CRB–AT–ARB3, and CRB–AT–ARB5 samples



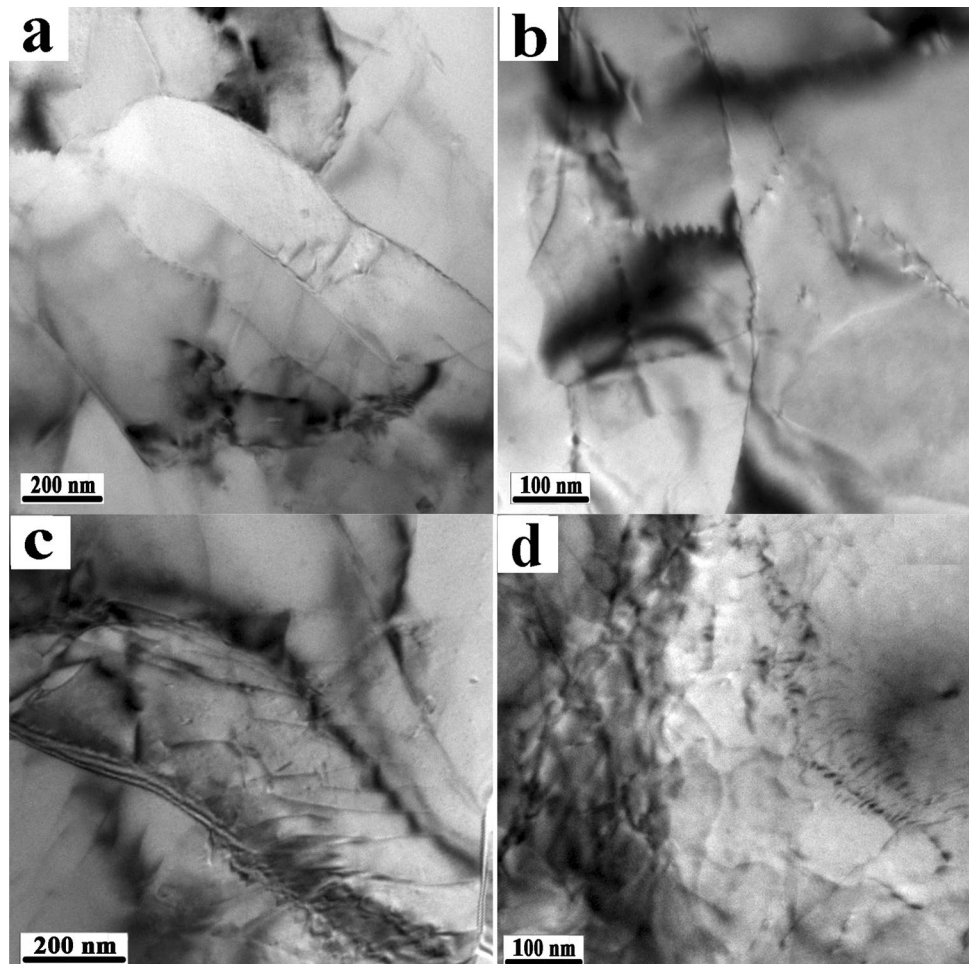
the intensity of α fiber increases and reaches its maximum value after five cycles.

To investigate the changes in the intensity of different texture components in different samples, the intensities of important components were calculated. The variations in the intensity of different texture components are presented in Fig. 8. For simplification, the sum of intensities of recrystallization texture components R5, P, Q, and R was considered equal to Rex. Changes in the Rex component indicate that the recrystallization texture present in the initial Al was relatively large, about $13 \times R$. After CRB, this texture component became weak and reached about $5 \times R$; however, after annealing, it again increased sharply and reached an intensity of $24 \times R$. The subsequent ARB cycles reduced the intensity of the Rex recrystallization texture component; its value was $5 \times R$, after one ARB cycle, and it was very small and close to zero after five ARB cycles. The Goss and Brass rolling texture components, which were created after CRB, were significantly weakened by annealing and were strengthened once more throughout the ARB process in the sample. The intensity of Goss, Copper, Brass, Dillamore, and S components increased with increase in ARB cycles. With increase in strain from the first to fifth ARB cycle, the intensity of the Goss component changes from $2 \times R$ to $30 \times R$. For the Copper, Dillamore, and S components, these values change from $2 \times R$ to $6 \times R$, $1.5 \times R$ to $4.5 \times R$, and $2 \times R$ to $4 \times R$, respectively. Numerous earlier research have observed and reported an increase in rolling texture component intensity with increasing strain. For example, Roy et al. (2011) found that by performing the ARB process on the Al 5086 alloy, a large number of the deformation texture components were amplified in comparison to that in the initial

material. The recrystallization components were preserved during the ARB process. Past research has shown that in Al, due to annealing after roll bonding, a cubic texture develops similar to the texture of metals with moderate to high stacking fault energy (Humphreys and Hatherly 2004). Examination of changes in the intensity of cube and rotated cube components showed that the intensity of these texture components in the CRB–AT sample was very low ($1 \times R$). The reason for the low intensity of this sample is probably the presence of secondary phase particles (Hutchinson 2012). In this sample, with increase in ARB cycles, cubic texture intensity also increased, and, in the CRB–AT–ARB3 sample, it reached its maximum value, i.e., $2 \times R$; however, the intensity of this texture component in the composite sample containing TiAl_3 reinforcement particles was minimal after five cycles of ARB.

A noteworthy point in these results is the elimination of the cubic texture component in the structure after the third cycle of ARB. The reason for this occurrence is the formation of shear bands (Humphreys and Hatherly 2004). In FCC materials with moderate to high stacking fault energy and in materials containing coherent second-phase particles, shear bands are formed due to differences in plasticity between the matrix and the reinforcement particles (Quadir et al. 2009). While there is no shear bands in CRB–AT–ARB3 sample (Fig. 9a, b), nano shear bands are observed in the TEM images of the final sample (CRB–AT–ARB5) in Fig. 9c, d. Shear bands intersect the elongated cube bands, and thus, prevent the formation of cubic texture (Humphreys and Hatherly 2004). However, the appearance of shear bands can change the deformation texture. Shear bands tend to cause the rotation of the material in the transverse direction (TD),

Fig. 9 TEM images related to **a, b** CRB–AT–ARB3 and **c, d** formation of nano shear bands in the CRB–AT–ARB5 sample at two different magnifications



which can contribute to changes in texture intensity and intensity redistribution along with the β fiber. In particular, shear bands strengthen the components of Goss and Brass (Lucke and Engler 1990).

The pole figure images of the (111) plane and the ODF images in sections φ_2 equal to 45°, 65°, and 90° corresponding to the initial Al, CRB, CRB–ARB1–AT, CRB–ARB3–AT, and CRB–ARB5–AT samples are demonstrated in Figs. 10 and 11, respectively. Figure 10a shows that initial Al has R5 and Q recrystallization texture components. It also contains the S component, a rolling texture component related to the deformation effects of initial Al before annealing. As shown in Fig. 11a, the ODF images of the initial Al specimen confirm recrystallization texture. The (111) pole figure image of the CRB sample in Fig. 10b shows the formation of a rolling texture composed of Copper and Goss components. The S component is also amplified in this sample. Among the recrystallization texture components, only the R5 recrystallization component is present after CRB with a slight decrease in intensity. The ODF images of this sample (Fig. 11b) show the formation of the Goss component, one of the components of α fiber (in the section φ_2

equal to 90°). According to Fig. 10c, performing one cycle of ARB after CRB (CRB–ARB) has resulted in the formation of Goss, Brass, Copper, S, cube, and rotated cube components. Moreover, recrystallization texture components are still present in the structure. The ODF images of this sample are presented in Fig. 11c, which show that α and β fibers were formed after ARB. According to Fig. 10d, annealing after CRB and one cycle of ARB (CRB–ARB1–AT) has resulted in the strengthening of the recrystallization texture and the intensification of the R5 and R components. Contrary to the CRB–AT sample (Fig. 6c), the P recrystallization component was not formed in this sample; this shows that the decline in the second-phase particle size in this sample due to the first ARB cycle has reduced the intensity of the P recrystallization texture. The ODF images of this sample are presented in Fig. 11d and show the disappearance of the rolling texture components and the formation of areas with recrystallization texture. Moreover, the fibers have been destroyed by annealing. The cube component has a very low intensity in this sample. The (111) pole figure image of the CRB–ARB3–AT sample is shown in Fig. 10e. The prominent recrystallization texture components in this

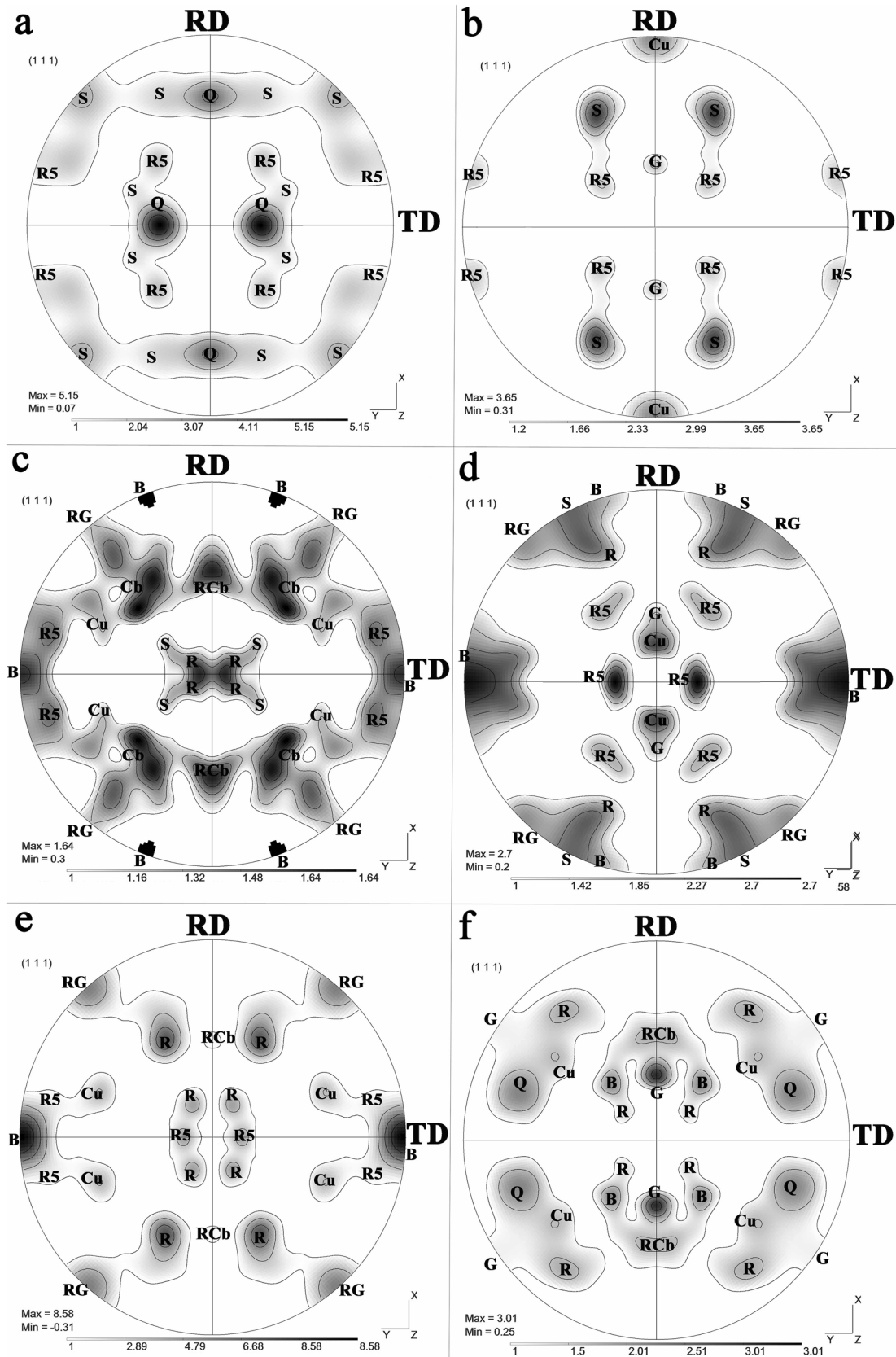


Fig. 10 (111) pole figure images of RD-TD cross-section obtained from EBSD test related to **a** initial Al, and **b** CRB, **c** CRB-ARB1, **d** CRB-ARB1-AT, **e** CRB-ARB3-AT, and **f** CRB-ARB5-AT samples

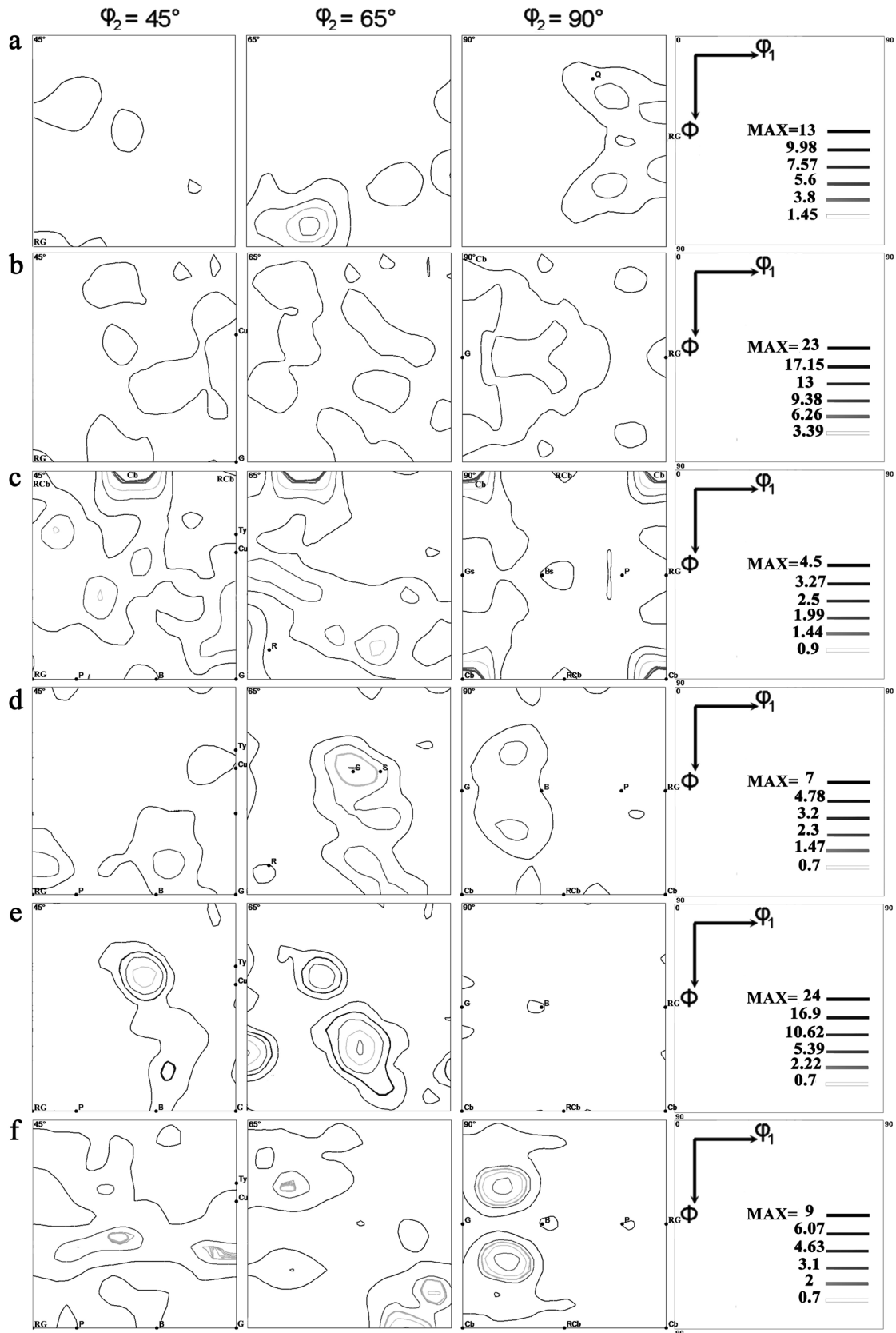


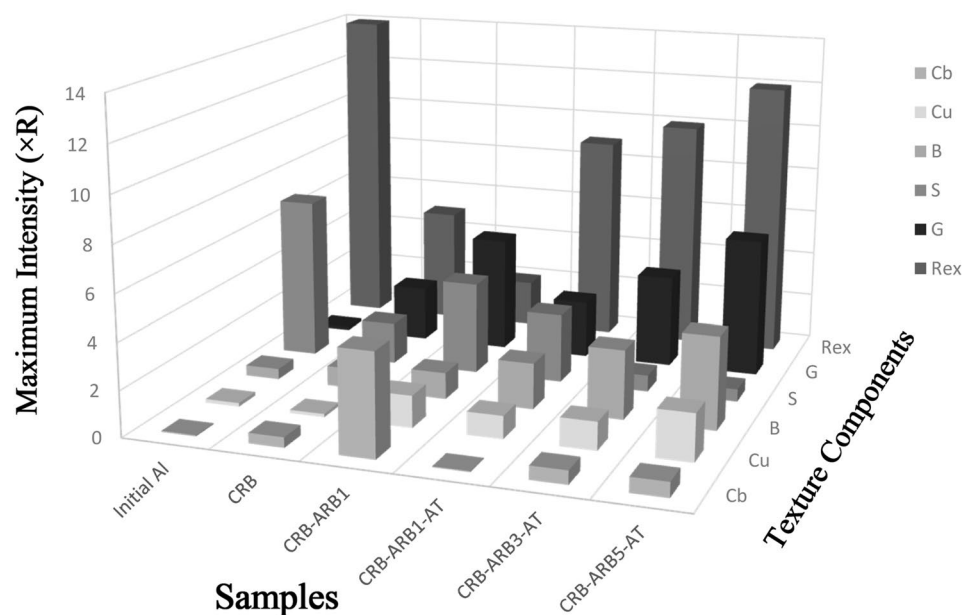
Fig. 11 ODF images in sections ϕ_2 equal to 45° , 65° , and 90° related to the RD-TD plane obtained from EBSD test related to **a** initial Al, and **b** CRB, **c** CRB-ARB1, **d** CRB-ARB1-AT, **e** CRB-ARB3-AT, and **f** CRB-ARB5-AT samples

sample include R and R5. Thus, the intensity of the rolling texture components is reduced, and the S component is almost eliminated. This image also shows the presence of a rotated cube component with low intensity. The ODF results shown in Fig. 11e also confirm the elimination of the rolling texture components and the development of the recrystallization texture components. Furthermore, the Brass component in this sample showed a more significant decrease than that in the CRB–ARB1–AT sample. Finally, the pole figure image of the CRB–ARB5–AT sample is shown in Fig. 10f. According to this image, the rotated cubic texture component is reinforced. Recrystallization texture components R, R5, and Q are also generated by annealing. The ODF images in Fig. 11f show the increased intensity of the Copper component and the complete elimination of the S component in this sample. The intensity of Goss and Brass components decreased more significantly in this sample than in the other two samples (Fig. 11d, e).

To study the texture changes in different stages, the intensity of essential components was calculated and the intensity changes are shown in Fig. 12. To simplify, the total intensities of recrystallization texture R5, Q, and R were considered equal to R_{ex} . Changes in the R_{ex} recrystallization texture component indicate that the recrystallization texture present in the initial Al is relatively large, about $14 \times R$. Due to CRB, this texture weakened and reached about $5 \times R$. The subsequent ARB cycle further reduced the intensity of the R_{ex} recrystallization texture to $2 \times R$. Annealing after one, three, and five cycles of ARB resulted in a rise in the R_{ex} recrystallization component to values of $9 \times R$, $10 \times R$, and $12 \times R$, respectively. The contribution of the annealing-induced recrystallization component was increased with increase in the number of ARB cycles. Comparison of the intensities of

Goss, Copper, and Brass components in CRB–ARB1–AT, CRB–ARB3–AT, and CRB–ARB5–AT samples shows that with increase in pre-annealing strain, these components have become more intense and have the values of $2.5 \times R$, $1 \times R$, and $2 \times R$, respectively, due to annealing after the first cycle, and values of $6 \times R$, $2 \times R$, and $4 \times R$ due to annealing after the fifth cycle. A noteworthy point is the elimination of the S component due to annealing after the third and fifth cycles of ARB. Previous reports have shown that the presence of the S component in FCC materials leads to the appearance of a cube component in the recrystallization texture. The formation of the cube component during the recrystallization of roll bonded Al is a common phenomenon. Due to the $40^\circ \langle 111 \rangle$ orientation relationship between the cube component and S component, researchers believe that the cause of the cubic recrystallization texture is the presence of S component, and the intensity of the S component decreases because of the annealing treatment after rolling (Lee and Han 2014). According to previous research, it is expected that with increase in the number of ARB cycles after annealing, as the intensity of component S decreases, the intensity of cube and rotated cube components increases and strengthens in high thickness reduction in rolling (Humphreys and Hatherly 2004). Although, in these composite samples, due to the presence of $TiAl_3$ reinforcement particles and the formation of shear bands due to ARB, a weak cube component is formed. The values of the cube component increase with an increase in strain before annealing. Recrystallization nucleates in the shear bands and texture components such as Goss and recrystallization components are formed (Humphreys and Hatherly 2004). The increase in the intensity of Goss and Brass components after annealing with increase in the number of ARB cycles is also due to the presence of

Fig. 12 Values of important texture components in initial Al, and CRB, CRB–ARB1, CRB–ARB1–AT, CRB–ARB3–AT, and CRB–ARB5–AT samples



shear bands (Lucke and Engler 1990). In general, the existence of second-phase particles during deformation affects the recrystallization texture. Large particles (larger than 1 μm) already present in the material are suitable nucleation sites during recrystallization. Deformed areas with a large misorientation around them cause a wide range of grains directions. Moreover, the scattering of particles at close distances causes to lock of the grain boundaries, and affects recrystallization kinetics, texture, and the final grain size (Humphreys and Hatherly 2004).

In the CRB–AT–ARB sample, the final texture consisted of a rolling texture with a strong Goss component (about $30\times R$). In the CRB–ARB–AT sample, the final texture consisted of a random texture with a weaker Goss component (about $6\times R$) and a small amount of cube component. The metal texture has an essential effect on mechanical properties. For example, it has been reported that the presence of grains with Goss texture causes a crack deflection in the toughness test, while the Brass, Copper, and S components have little effect on crack initiation in this test. In addition, the ratio of the volume fraction of Goss component to Brass has a significant impact on the fracture toughness; the higher the ratio, the greater the fracture toughness of the material (Zhao et al. 2016). Furthermore, the cube component has a high anisotropy and results in a decline in mechanical properties. Nevertheless, the components of Goss, Brass, and Copper improve the mechanical properties. On the one hand, ARB before annealing, through the reduction of grain size and the development of rolling texture, results in smaller recrystallization grains and limited grain growth. On the other hand, by performing controlled annealing after the ARB process, a structure with a dual grain size distribution that offers a combination of appropriate strength and flexibility properties can be reached. However, due to the high annealing temperature in this study, which was selected due to the formation of intermetallic compounds, returning processes occurred extensively and led to the softening of the matrix and reduction of the matrix strength. In general, through the fabrication of Al-based composites with TiAl_3 intermetallic compound reinforcement particles through annealing, and then ARB, desirable properties can be achieved. The acquisition of intermetallic particles after ARB leads to the return of valuable properties due to severe plastic deformation.

Conclusion

In the present study, Al matrix composite with TiAl_3 reinforcement particles was obtained through different methods of CRB, and annealing of Al 1100 sheets, and pure Ti powder, and microstructural and texture evaluations were performed. The main results of this article are:

1. A maximum of five ARB cycles after annealing led to the fabrication of ultra-fine grain composite of about 500 nm containing a uniform distribution of TiAl_3 intermetallic compound particles with dimensions larger than 200 nm. The grain size of Al in the monolithic Al sample processed under the same conditions was about 700 nm.
2. The presence of reinforcement particles, by increasing dislocation densities and suitable places for nucleation of sub-grains in the Al matrix, further reduces the grain size of the matrix.
3. Annealing after CRB resulted in the strengthening of the recrystallization texture. Subsequent ARB cycles (maximum: five cycles) replaced the recrystallization texture components with deformation texture components, including Goss, Copper, Dillamore, Brass, and S.
4. Evaluation of the microstructure of composites fabricated through CRB–ARB–annealing method also showed that the grain size of Al obtained after these processes is within the micron range; in addition, the particle size of intermetallic compounds ranged from 0.2 to 50 μm .
5. Annealing after ARB leads to an increase in the recrystallization texture component. Moreover, the contribution of the annealing-induced recrystallization component has increased with increase in the number of ARB cycles.
6. Annealing before the ARB process caused the formation of a compact layer with few voids, while annealing after the ARB process increased the voids and created an equiaxed structure.

For future study, more accurate results will be achieved by investigating the effect of shear strain distribution on texture and evaluation of texture on the surface of the sheets.

Supplementary Information The online version contains supplementary material available at <https://doi.org/10.1007/s41403-023-00397-9>.

Declarations

Conflict of Interest The authors declare that they have no known competing financial interests or personal relationships that could have appeared to influence the work reported in this paper.

References

- Chaudhari GP, Acoff VL (2010) Titanium aluminide sheets made using roll bonding and reaction annealing. *Intermetallics* 18:472–478
- Heathcote J, Odette G, Lucas G, Rowe R, Skelly D (1996) On the micromechanics of low temperature strength and toughness of intermetallic/metallic microlaminate composites. *Acta Mater* 44:2489
- Humphreys FJ, Hatherly M (2004) *Recrystallization and related annealing phenomena*. Elsevier, Oxford

- Hutchinson B (2012) The cube texture revisited. *Mater Sci Forum* 702–703:3–10
- Jamaati R, Toroghinejad MR (2010) High-strength and highly-uniform composite produced by anodizing and accumulative roll bonding processes. *Mater Design* 31:4816–4822
- Jamaati R, Toroghinejad MR, Hoseini M, Szpunar JA (2011) Texture development in Al/Al₂O₃ MMCs produced by anodizing and ARB processes. *Mater Sci Eng A* 528:3573–3580
- Lee DN, Han HN (2014) The cube recrystallization-texture related component in the β -fiber rolling-texture FCC metals. *Mater Sci Forum* 783–786:51–56
- Lesuer D, Syn C (1994) Metallic laminates for engine applications, June–July 1994
- Liu CY, Jing R, Wang Q, Zhang B, Jia YZ, Ma MZ, Liu RP (2012) Fabrication of Al/Al₃Mg₂ composite by vacuum annealing and accumulative roll-bonding process. *Mater Sci Eng A* 558:510–516
- Loo FV, Rieck G (1973) Diffusion in the titanium-aluminum system-interdiffusion between solid Al and Ti or Ti-Al alloys. *Acta Metall* 21:61–71
- Lucke K, Engler O (1990) Effects of particles on development of microstructure and texture during rolling and recrystallisation in fcc alloys. *Mater Sci Technol* 6:1113–1130
- Luo JG, Acoff VL (2004) Using cold roll bonding and annealing to process Ti/Al multi-layered composites from elemental foils. *Mater Sci Eng A* 379:164–172
- Oh J, Pyo SG, Lee S, Kim NJ (2003) Fabrication of multilayered titanium aluminide sheets by self-propagating high-temperature synthesis reaction using hot rolling and heat treatment. *J Mater Sci* 38:3647–3651
- Quadir MZ, Ferry M, Al-Buhamad O, Munroe PR (2009) Shear banding and recrystallization texture development in a multilayered Al alloy sheet produced by accumulative roll bonding. *Acta Mater* 57:29–40
- Raei M, Toroghinejad MR, Jamaati R, Szpunar JA (2010) Effect of ARB process on textural evolution of AA1100 aluminum alloy. *Mater Sci Eng A* 527:7068–7073
- Rana RS, Purohit R, Das S (2012) Review of recent studies in Al matrix composites. *Int J Sci Eng Res* 3:1–16
- Roy S, Singh S, Suwas DS, Kumar S, Chattopadhyay K (2011) Microstructure and texture evolution during accumulative roll bonding of aluminium alloy AA5086. *Mater Sci Eng A* 528:8469–8478
- Saito Y, Tsuji N, Utsunomiya H, Sakai T, Hong RG (1998) Ultra-fine grained bulk aluminum produced by accumulative roll-bonding (ARB) process. *Scr Mater* 39:1221–1227
- Saito Y, Utsunomiya H, Tsuji N, Sakai T (1999) Novel ultra-high straining process for bulk materials development of the accumulative roll-bonding (ARB) process. *Acta Mater* 47:579–583
- Sieber H, Perepezko JH (2000) Intermetallic phase formation in bulk multilayered structures. In: Morris DG, Naka S, Caron P (eds) *Intermetallics and superalloys*. WILEY-VCH Verlag GmbH, New York, pp 324–329
- Smallman RE, Bishop RJ (1999) *Mechanical behaviour of materials, Modern physical metallurgy and materials engineering*, 6th edn. Butterworth-Heinemann, Oxford, pp 197–258
- Tsuji N, Ito Y, Saito Y, Minamino Y (2002) Strength and ductility of ultrafine grained aluminum and iron produced by ARB and annealing. *Scr Mater* 47:893–899
- Yang DK, Hodgson P, Cui EW (2009) The kinetics of two-stage formation of TiAl₃ in multilayered Ti/Al foils prepared by accumulative roll bonding. *Intermetallics* 17:727–732
- Yazdani Z, Toroghinejad MR, Edris H, Ngan AHW (2018a) A novel method for the fabrication of Al-matrix nanocomposites reinforced by mono-dispersed TiAl₃ intermetallic via a three-step process of cold-roll bonding, heat-treatment and accumulative roll bonding. *J Alloys Compd* 747:217–226
- Yazdani Z, Toroghinejad MR, Edris H, Ngan AHW (2018b) Effect of cold rolling parameters on bond strength of Ti particle embedded Al strips. *Trans Indian Inst Metals* 71:2497–2504
- Zhang L, Wang Y, Yang X, Li K, Ni S, Du Y, Song M (2017) Texture, microstructure and mechanical properties of 6111 aluminum alloy subject to rolling deformation. *Mater Res* 20:1360–1368
- Zhao Q, Liu Z, Huang T (2016) Enhanced fracture toughness in an annealed Al–Cu–Mg alloy by increasing Goss/Brass texture ratio. *Mater Charact* 119:47–54

Publisher's Note Springer Nature remains neutral with regard to jurisdictional claims in published maps and institutional affiliations.

Springer Nature or its licensor (e.g. a society or other partner) holds exclusive rights to this article under a publishing agreement with the author(s) or other rightsholder(s); author self-archiving of the accepted manuscript version of this article is solely governed by the terms of such publishing agreement and applicable law.